3D-Printed Peptide-Hydrogel Nanoparticle Composites for Surface-Enhanced Raman Spectroscopy Sensing

Sawsan Almohammed,[a, b] Maha Alruwaili,[a, b] Emmanuel G. Reynaud,[b, c] Gareth Redmond,[d] James H. Rice[a]* and Brian J. Rodriguez[a, b]*

[a]School of Physics, University College Dublin, Belfield, Dublin 4, Ireland
[b]Conway Institute of Biomolecular and Biomedical Research, University College Dublin, Belfield, Dublin 4, Ireland
[c]School of Biomolecular and Biomedical Science, University College Dublin, Belfield, Dublin 4, Ireland
[d]School of Chemistry, University College Dublin, Belfield, Dublin 4, Ireland

*James.Rice@ucd.ie and Brian.Rodriguez@ucd.ie

ABSTRACT: Precise control over the arrangement of plasmonic nanomaterials is critical for label-free single-molecule surface-enhanced Raman spectroscopy (SERS)-based sensing applications. SERS templates should provide high sensitivity and reproducibility and be cost-effective and easy to prepare. Additive manufacturing by extrusion-based 3 dimensional (3D) printing is an emerging technique for the spatial arrangement of nanomaterials and is a method that may satisfy these SERS template requirements. In this work, we use 3D printing to produce sensitive and reproducible SERS templates using a fluorenylmethyloxycarbonyl diphenylalanine (Fmoc-FF) hydrogel loaded with silver or gold nanoparticles. The Fmoc-FF template allows the detection of low Raman cross-section molecules such as adenine at concentrations as low as 100 pM.

Keywords: 3D bioprinting, additive manufacturing, peptides, Fmoc, diphenylalanine, Raman, SERS, SERRS

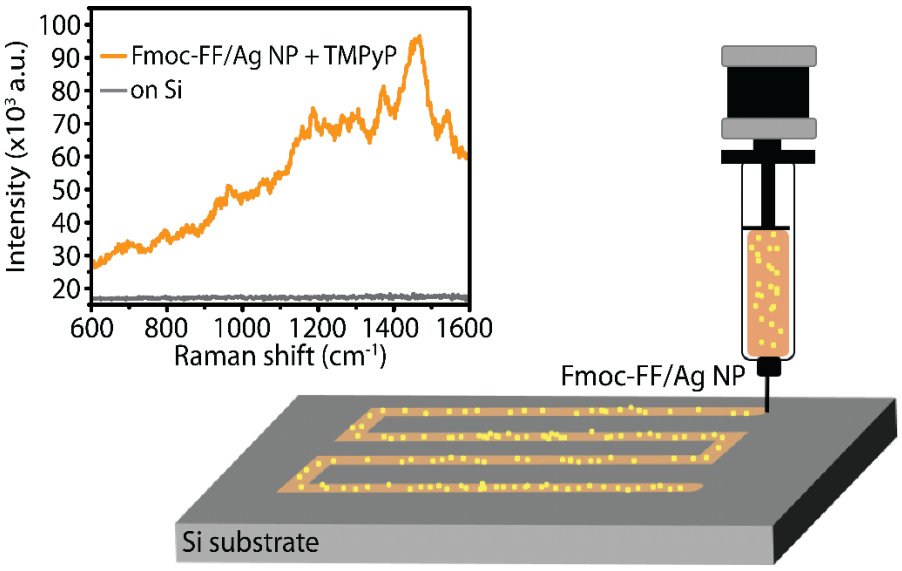

INTRODUCTION

Hydrogels are of great interest as a class of materials for tissue engineering and wound healing.[1] Hydrogels that incorporate nanoparticles (NPs) provide a route to tailor the functionality of the nanocomposite, further enabling a variety of biomedical applications, including biomolecular sensing.[2] In the past decade, peptide-based hydrogels, most notably fluorenylmethoxycarbonyl-diphenylalanine (Fmoc-FF), have gained attention for their self-assembly of fibrous structures via π–π stacking of β-sheets that give rise to a biocompatible, nanofibrous mimic of an extracellular matrix.[3–10] Peptide–metal NP composites, in particular, have been used for drug delivery and electrochemical biosensing applications,[11–13] and more recently, in surface-enhanced Raman spectroscopy (SERS)-based sensing applications using FF-nanotube–metal NP composites.[14–16] Although nanoparticles and organic-nanoparticle composites that may facilitate cellular and biomolecular sensing applications have been assembled through bio-templating and self-assembly routes,[14,16,25–31,17–24] few of these have been used for SERS,[14,16–19,25,28,29,31] and none are based on Fmoc-FF.

The fabrication of highly sensitive, reproducible, stable, and cost-effective SERS templates remains an actively-researched topic.[32–34] Several potential solutions to these issues have been investigated, including the use of alumina masks[35] and ink jet printing[36–40] to allow the location of SERS-active regions to be spatially defined. Furthermore, 3D SERS templates have gained interest recently as a means to provide a larger surface area for increased analyte capture and to exploit the focal volume of the Raman excitation laser. By increasing the number of hotspots in the z-direction, the Raman signal can be increased and detection limits can be lowered.[41–44]

Extrusion-based 3D printing is a direct deposition additive manufacturing approach that enables the layer-by-layer deposition of materials in x, y, and z to fabricate multilayer 3D structures. 3D printing has been used previously for the deposition of hydrogels and hydrogel–NP composites.[45] The ability to deposit nanomaterials in a spatially controlled fashion is key to the fabrication of large-scale, reproducible templates for flexible electronics and integrated biosensing devices using additive manufacturing approaches.[46–49] Furthermore, 3D printing has been reported to lead to shear induced alignment of nanofibers within a hydrogel[50] and may therefore provide a suitable templating or confinement effect that results in a closely packed arrangement of nanostructures and NPs. Hydrophobic-hydrophilic interfaces have previously been used to simultaneously align FF nanotubes and confine NPs for SERS applications.[15]

In this work, we assess whether a biocompatible nanofibrous Fmoc-FF peptide gel combined with metal NPs can serve as a SERS template when 3D printed. We establish the suitability of 3D printing for the fabrication of Fmoc-FF hydrogel–metal NP composite SERS templates by detecting molecules at concentrations as low as 1 pM for a molecule in resonance with the laser excitation wavelength used and as low as 100 pM for a non-resonant molecule.

MATERIALS AND METHODS

Fmoc-FF hydrogel preparation

Fmoc−FF (B2150, Bachem AG) was dissolved in dimethyl sulfoxide (DMSO) (472301, Sigma-Aldrich) at a concentration of 100 mg/ml. The resulting solution was diluted in double distilled water (ddH_2O) to a final concentration of 2 mg/ml (unless stated otherwise). Upon mixing with water, the opaque solution began to gel and eventually became translucent over the course of ~ 4 mins as nanofibers formed (Fig. S1).

Fmoc-FF/Ag NP and Fmoc-FF/Au NP hydrogel preparation

Ag NP-loaded Fmoc-FF hydrogels were prepared by adding 2 ml of 40 nm diameter Ag NP solution (0.02 mg/ml in water; 795968, Sigma-Aldrich) to 2 ml of 2 mg/ml of Fmoc-FF solution prior to hydrogel formation (Fmoc-FF:Ag NP volume ratio of 1:1) unless otherwise specified. The Fmoc-FF/Ag NP hydrogel preparation is shown schematically in Fig. 1. Similarly, Au NPs (765546, Sigma-Aldrich) with a diameter of 40 nm at a concentration of 0.02 mg/ml in water were used to prepare Fmoc-FF/Au NP hydrogels with a Fmoc-FF:Au NP volume ratio of 1:1. In both cases, gelation took place over the course of ~ 4 mins. The hydrogels were heated for ~ 5 mins at 100 °C and left to cool for ~ 10 mins prior to use.

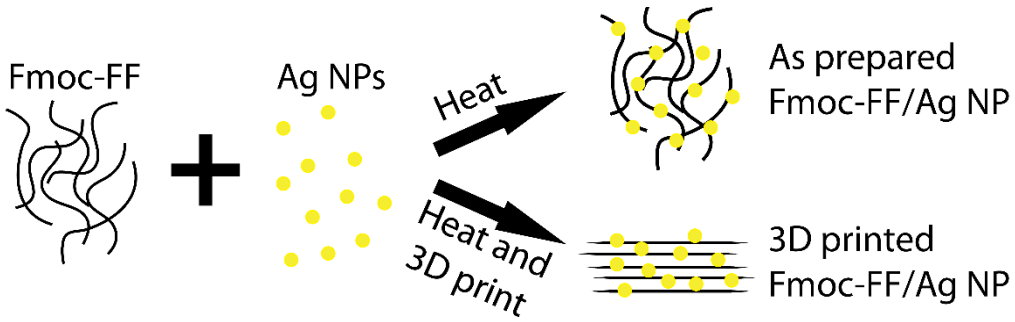

Figure 1. Schematic showing the preparation of as prepared and 3D printed Fmoc-FF/Ag NP hydrogels. Fmoc-FF/Ag NP hydrogels are prepared by adding Fmoc-FF and 40 nm diameter Ag NPs. After gelation, the solution is heated for ~ 5 mins at 100 °C to promote mixing and to facilitate deposition. After cooling for ~ 10 minutes Fmoc-FF/Ag NP hydrogels were deposited via pipette onto a glass or Si substrate (as prepared) and 3D printed onto glass or Si.

3D printing of Fmoc-FF templates

The 3D printer used consisted of an Ultimaker 1.0 frame and axes, which had been converted to a stepper motor-driven syringe-based extrusion system.[51] A bespoke raster-pattern G-code was written to define the print head path, extrusion parameters, and final printed structure, shown schematically in Fig. 2. The Fmoc-FF hydrogel with and without NPs was printed using a flat-end plastic tip (Somerset Solders Ltd, UK) with a nozzle diameter of 0.4 mm with a distance of 0.2 mm between the nozzle and the substrate.

Preparation of probe molecule solutions

Meso-tetra (N-methyl-4-pyridyl) porphine tetrachloride (TMPyP) (T40125, Frontier Scientific) and adenine (A8626, Sigma-Aldrich) were diluted with ddH_2O to concentrations ranging from 10^{-4} – 10^{-11} M and 10^{-4} – 10^{-10} M, respectively.

Ultraviolet–visible (UV-Vis) spectroscopy

Optical absorbance measurements of Fmoc-FF with and without Ag (or Au) NPs and also of the analyte molecules were performed using UV-Vis (V-650, JASCO, Inc.) under identical settings: 1 nm step size, 1 nm bandwidth, and 400 nm/min scan speed across a 190 – 900 nm range. A quartz cuvette or glass cover slip was used to conduct the measurements.

Fourier transform infrared (FTIR) spectroscopy

FTIR measurements were performed using an FTIR spectrometer (Alpha Platinum ATR, Bruker). 10 µl of Fmoc-FF with and without Ag NPs was placed on the attenuated total reflection diamond crystal. The spectrum was collected using transmission mode, scanning from 1400 – 4000 nm.

Scanning electron microscopy (SEM)

SEM (JSM-7600F, JEOL, operated at 5 kV) was employed to characterize Fmoc-FF and observe the location of NPs. Approximately 8 nm layer of gold was sputtered (Hummer IV, Anatech USA) on the samples prior to SEM.

Raman spectroscopy

SERS measurements were performed using a bespoke Raman system comprising an inverted optical microscope (IX71, Olympus) with a 50x, 0.42 numerical aperture objective used to focus the 532 nm, 5 mW incident power laser (ThorLabs) to a spot size of ~ 10 µm,[52] a beam splitter and a long pass filter (RazorEdge, Semrock), a spectrograph (SP-2300i, Princeton Instruments), and a CCD camera (IXON, Andor). Raman spectra were collected with an exposure time of 1 s. 60 µl of TMPyP or adenine, at specified concentrations, was deposited on the Fmoc-FF/Ag NP templates. To characterize Raman signal uniformity, SERS measurements were performed at different locations on the printed structures. Raman measurements were also performed on DMSO and Fmoc-FF powder (B2150, Bachem AG) controls. To characterize sample variability, SERS measurements were performed on at least six different samples for each concentration. SERS measurements were also performed on Ag or Au NPs on Si. 200 µl of Ag or Au NP solution (0.02 mg/ml) was diluted in 2 ml of ddH_2O (to a final concentration of 0.002 mg/ml) and then 80 µl was deposited onto a Si substrate. After allowing the solution to dry, 60 µl of TMPyP or adenine was deposited onto the NPs on Si. The mean value of typically 10 measurements, is reported. Toluene was used to calibrate the Raman signal over the spectral window.

Optical microscopy

Optical profilometry (NT1100, Wyko) was used to image the hydrogels with and without NPs using a 10x objective.

RESULTS AND DISCUSSION

As prepared and 3D printed Fmoc-FF hydrogels with and without Ag NPs were imaged using SEM (Fig. 2) and optical microscopy (Fig. S2a). The snaking raster print shape is evident in Figs. 2a and S2a. The width of the printed line was measured to be 1.8 ± 0.2 mm (mean value of eight measurements from the print shown in the inset of Fig. 2a). The broadening of the line width compared to the 0.4 mm nozzle diameter can be attributed to the 0.2 mm distance between nozzle and substrate used. The as prepared hydrogels exhibited a dense network of fibrous structures with diameters of 101 ± 42 nm (n = 30 fibrils) in the absence of NPs (Fig. 2c). Fiber formation was apparently affected by the presence of NPs (Fig. 2d), resulting in a larger distribution of fibril widths and a larger mean fibril width (237 ± 129 nm; n = 30 fibrils). Shear induced alignment of the Fmoc-FF hydrogel was apparent from the 3D printed Fmoc-FF structure (Fig. 2c), wherein fibrils with diameters of 85 ± 32 nm (n = 30 fibrils) aligned along the print direction (see also Fig. S2). In the presence of NPs, fibrils with diameters of 86 ± 38 nm (n = 30 fibrils) decorated with NPs are observed at high magnification (Fig. 2d).

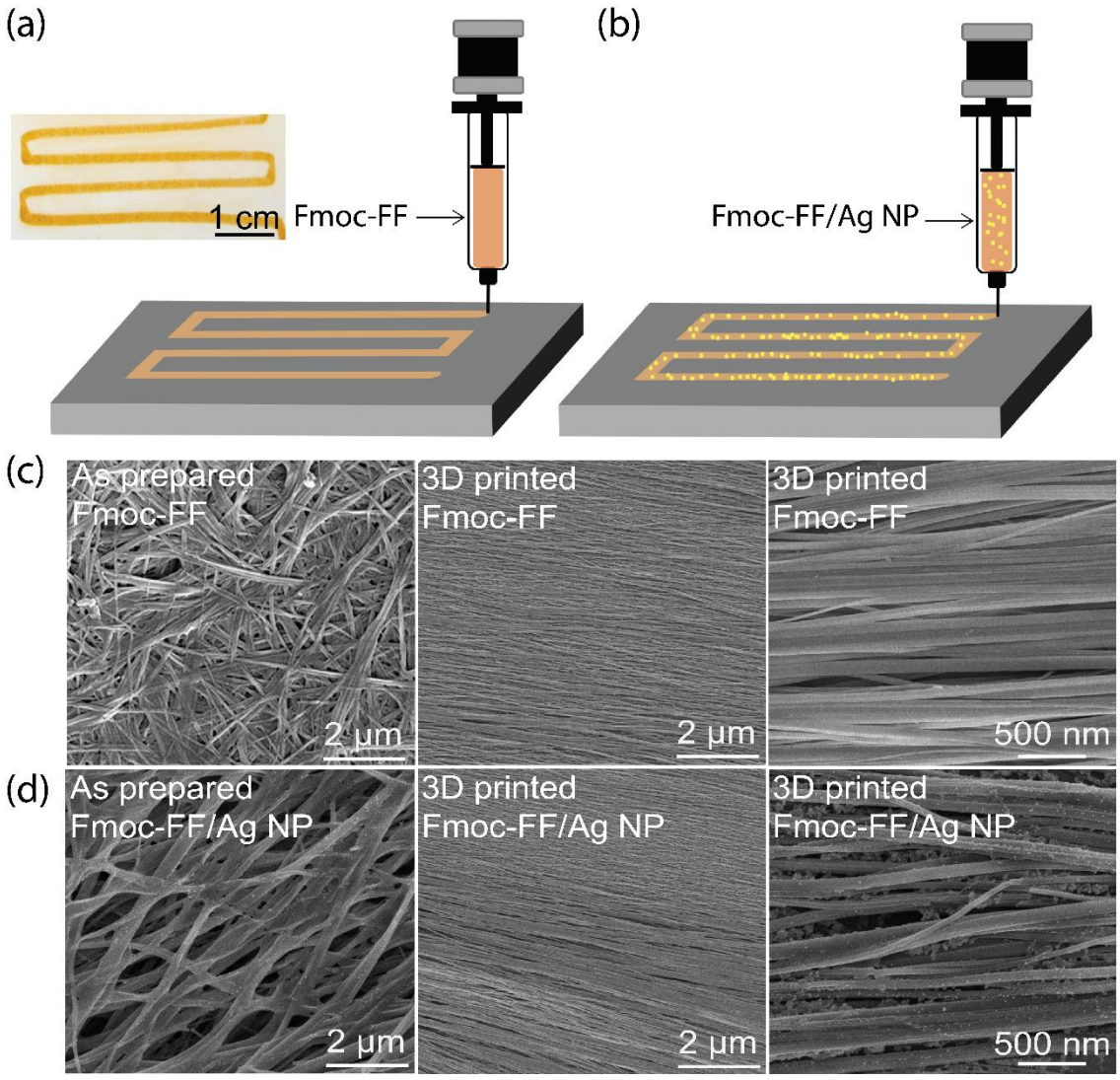

Figure 2. Schematic representation of the 3D printed hydrogel (a) without and (b) with NPs. The inset in (a) is an optical image of the hydrogel (mixed with 0.06 g of orange food dye (U8-OSL0-PS8Q, Preema, UK)) printed on glass. (c) SEM images of the as prepared and 3D printed Fmoc-FF. (d) SEM images of the as prepared and 3D printed Fmoc-FF with Ag NPs. Dye was used only for the inset in (a).

UV-Vis (Fig. S3) and FTIR (Fig. S4) spectroscopy were used to characterize the optical properties of Fmoc-FF with and without Ag NPs. Fmoc-FF exhibited pronounced absorption between 250 and 300 nm, accompanied by a peak at ~ 314 nm, in agreement with literature values.[1–3] Ag NPs alone exhibited a broad surface plasmon resonance peak at ~ 420 nm (full width at half maximum of ~ 72.5 nm). In combined Fmoc-FF/Ag NP solutions, the surface plasmon resonance band arising from Ag NPs was red-shifted by ~ 15 nm and narrowed by ~ 32 nm (Fig. S3), indicative of an interaction (e.g., adsorption or binding) between Fmoc-FF and NPs.[5,14–16] Sharp amide I absorption bands at 1674 and 1659 cm^{-1}, consistent with β-sheet and β-turn conformations were observed in the FTIR spectra of Fmoc-FF hydrogels both in the

presence and absence of NPs (Fig. S4). A band at 1739 cm^{-1}, corresponding to C=O stretching, appeared for Fmoc-FF with Ag NPs, presumably caused by the residual citrate stabilizing groups previously observed on Ag NPs.[1–3,5]

Ag NP loading increased with the volume of Ag NP solution used, as shown in SEM images (Fig. S5). At the same time, the Fmoc-FF fiber density could be controlled by changing the Fmoc-FF concentration in the range 0.5 mg/ml to 2 mg/ml (Fig. S5). Raman signals increased with increasing volume of NP solution used (Fig. S6a). The enhancement is attributed to the localized surface plasmon resonance of the NPs.[32–34] Bands associated with Fmoc-FF powder (Fig. S6b) were present (and enhanced by ~ 40 %) from the Fmoc-3D printed FF/Ag NP template, including the breathing modes at 998 and 1020 cm^{-1}, indicated with green shading in Fig. S6b, and other characteristic bands (719, 736, 1265, 1350, 1412, 1452 and 1507 cm^{-1}).[1–3] For as prepared Fmoc-FF, in contrast, mainly bands associated with DMSO were seen (682 and 713 cm^{-1}), highlighted with gray shading in Fig. S6b. Following the introduction of Ag NPs to as prepared Fmoc-FF, the breathing mode Fmoc-FF bands at 998 and 1020 cm^{-1} were more readily resolved.

Raman scattering measurements of the 3D printed Fmoc-FF/Ag NP templates were undertaken with a TMPyP probe molecule added at a range of concentrations from 10^{-4} M to 10^{-9} M (Fig. 3a). As above, in the absence of TMPyP, Fmoc-FF bands were present (Fig. 3a). An excitation wavelength of 532 nm was used, which is in resonance with the Q band of TMPyP (Fig. S7),[14–16] resulting in surface-enhanced resonance Raman scattering (SERRS). SERRS from TMPyP (C–C stretching band at 1452 cm^{-1}) increased with increasing concentration (Fig. 3a). SERRS intensity was higher from TMPyP on the 3D printed Fmoc-FF/Ag NP template compared to Ag NPs on Si for 10^{-6} M TMPyP, as shown in the inset of Fig. 3a. Negligible SERRS peaks from 10^{-10} M TMPyP were detected from a Si substrate with Ag NPs; however, intense characteristic Raman peaks of TMPyP at the same concentration were observed for the Fmoc-FF/Ag NP template (Fig. 3b). When the TMPyP solution was further diluted to 10^{-11} and 10^{-12} M, characteristic peaks, e.g., the 1452 cm^{-1} C–C stretching TMPyP band, were still visible. The enhancement observed from 3D printed Fmoc-FF/Ag NP templates compared to Ag NPs on Si is attributed to the stability of the 3D printed Fmoc-FF/Ag NP template upon addition of the TMPyP solution (Fig. S8) in contrast to the reduction in the number of NPs on the Si surface following the addition of TMPyP (Fig. S9).

Raman signals from TMPyP increased with increasing NP solution volume used and increased also with Fmoc-FF concentration (Fig. S10), consistent with the SEM images, which show that the Ag NPs aggregate primarily on Fmoc-FF fibers (Fig. S5). The results of Figs. S5, S6, and S10 support that increased NP loading into the gel was achieved with increasing volume of NP solution and that increased loading led to improved Raman intensity. Enhancement factors of the 1452 cm^{-1} peak similar to Fmoc-FF/Ag NP templates (~ 9 fold increase) have been obtained using 3D printed Fmoc-FF/Au NP templates (~ 8 fold increase), as shown in Fig. S11.

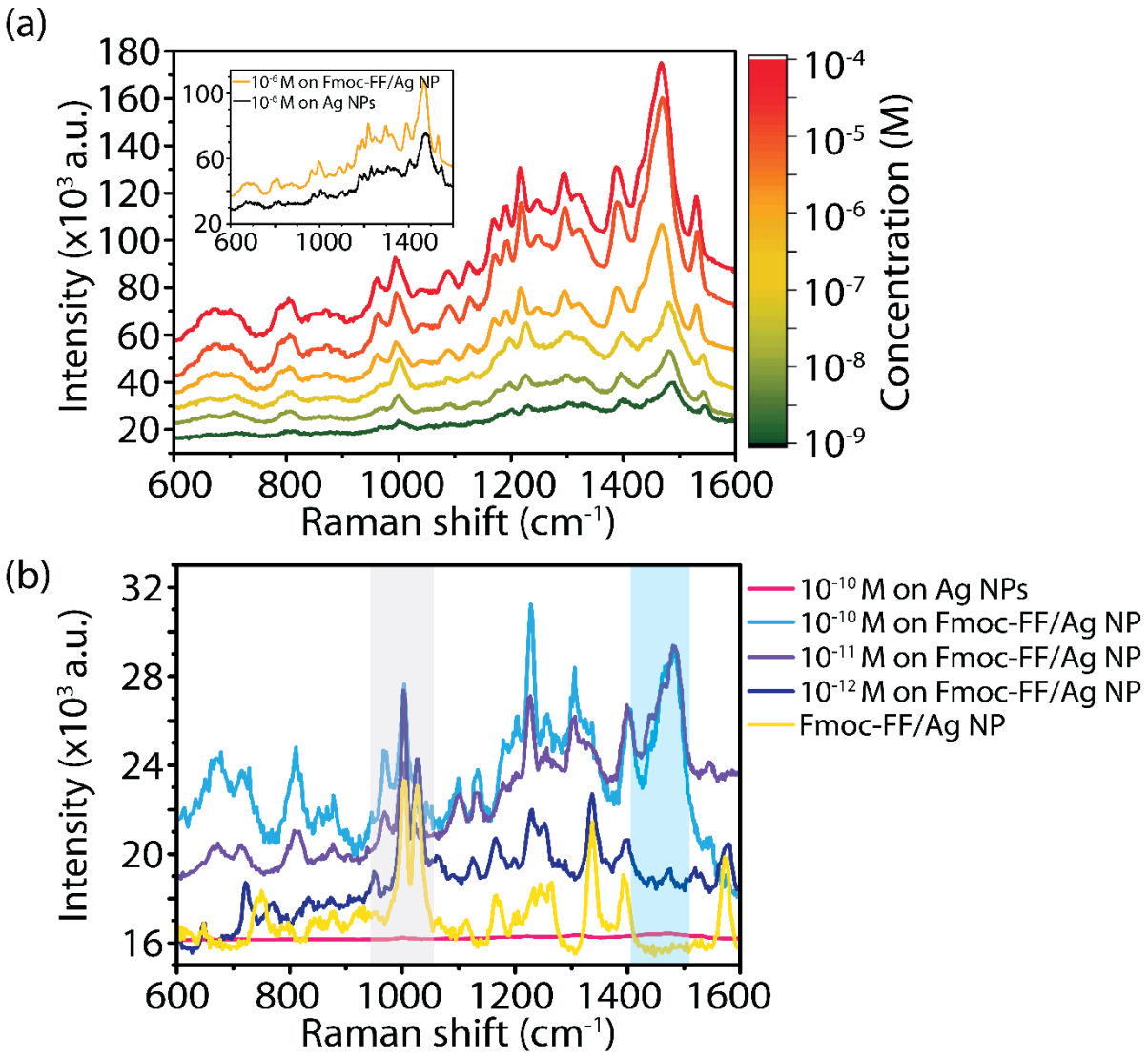

Figure 3. (a) SERRS spectra from TMPyP on the 3D printed Fmoc-FF/Ag NP template on Si at different concentrations. A comparison of SERRS intensity for 10^{-6} M TMPyP on 3D printed Fmoc-FF/Ag NP versus Ag NPs only is shown as an inset in (a). (b) SERRS spectra from 10^{-10}, 10^{-11}, and 10^{-12} M TMPyP on the printed template, from the template in the absence of TMPyP, and from 10^{-10} M TMPyP on Ag NPs alone. The gray shading in (b) corresponds to breathing mode bands of Fmoc-FF and the blue shading highlights the 1452 cm^{-1} C–C stretching TMPyP band.

The increased SERRS intensity from 3D printed Fmoc-FF/Ag NP templates compared to as prepared Fmoc-FF/Ag NP hydrogels might be attributed to a confinement effect provided by the shear induced alignment of the Fmoc-FF fibrils during 3D printing that increases the NP density (Fig S12). The Raman scattering intensity from TMPyP on Fmoc-FF/Ag NP templates increased linearly with increasing laser power, without decomposition (Fig. S13), allowing the detection of all bands associated with TMPyP. The Fmoc-FF template withstood laser powers

that generally lead to decomposition of TMPyP[53] on Ag NPs on Si, as shown by band broadening and disappearance in Fig. S13c.

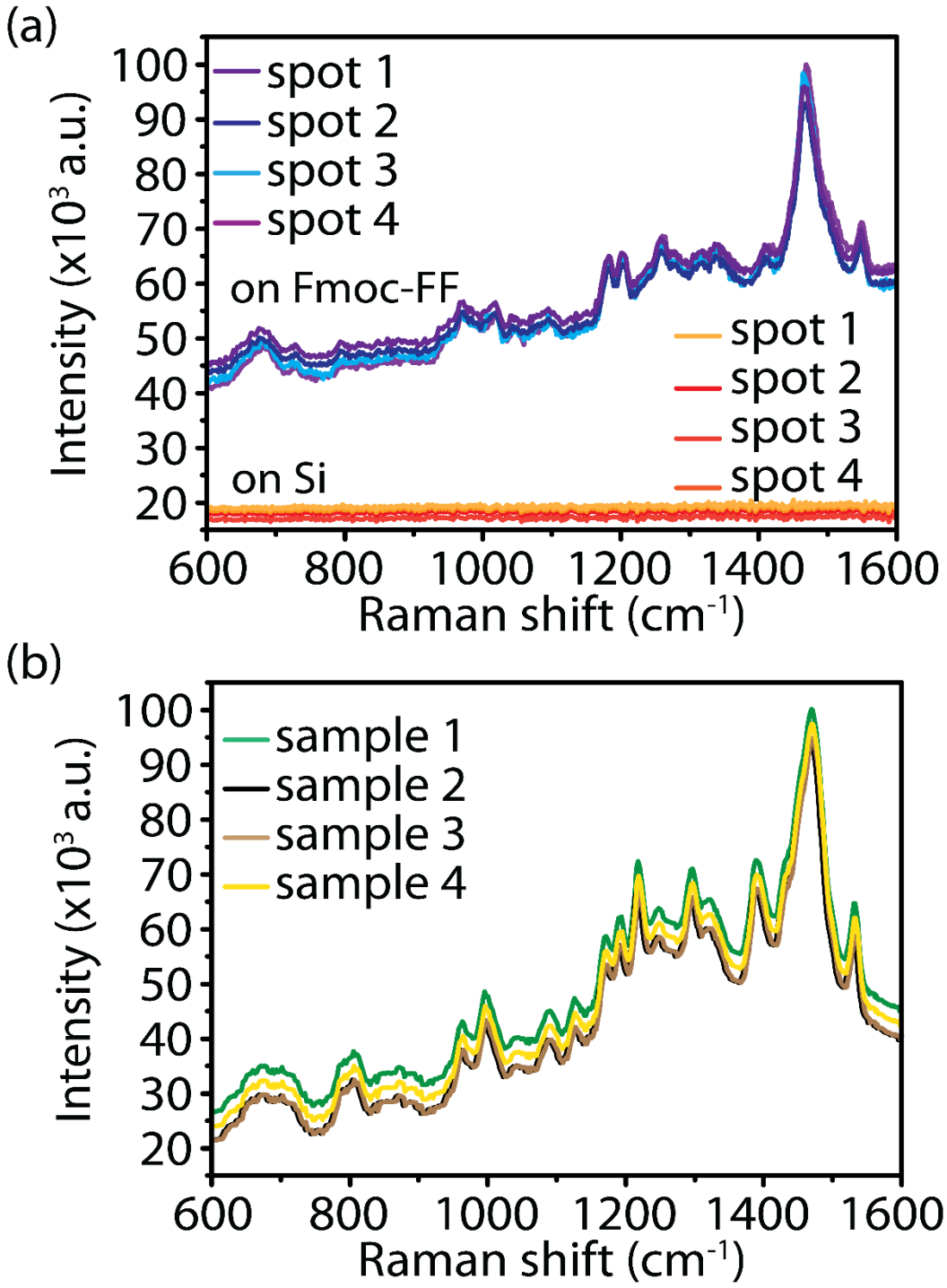

Figure 4. (a) SERRS spectra from 10^{-6} M TMPyP from different locations of the 3D printed Fmoc-FF/Ag NP template (on 3D printed Fmoc-FF/Ag NP and on adjacent Si regions). (b) SERRS spectra from 10^{-6} M TMPyP recorded from different 3D printed Fmoc-FF/Ag NP templates showing that the sample-to-sample variability is low.

Uniformity and reproducibility tests were conducted in different spots on a 3D printed Fmoc-FF/Ag NP hydrogel and on different templates (Fig. 4). SERRS signal uniformity is highlighted in Fig. 4a. The SERRS signal is present for TMPyP (10^{-6} M) on the 3D printed Fmoc-FF/Ag NP hydrogel and not on the Si surface, as expected, highlighting the applicability of 3D printing to control the location SERS-active materials. Reproducibility of the template was confirmed by recording SERRS spectra using 4 samples (Fig. 4b). Only ~ 5 % variation in SERRS intensity (for band at 1452 cm^{-1}) was seen for both uniformity and reproducibility studies, indicating low inter and intra sample variability.

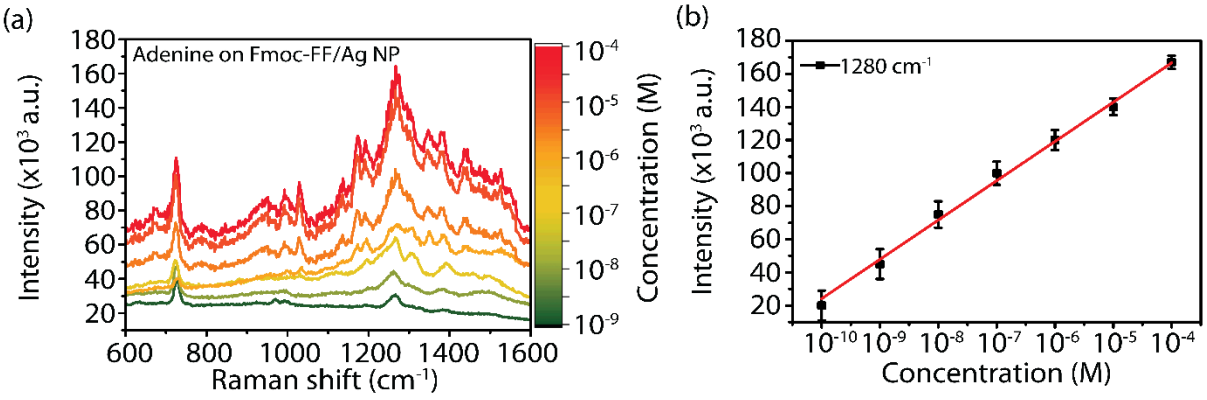

Figure 5. (a) SERS spectra from adenine on 3D printed Fmoc-FF/Ag NP templates at different adenine concentrations. (b) Plot and linear fit of SERS intensity of adenine band at 1280 cm^{-1} as a function of concentration.

To further demonstrate the applicability of the Fmoc-FF/Ag NP template for SERS detection, adenine, a non-resonant molecule, with absorption at ~ 280 nm (Fig. S7),[14–16] was investigated (Fig. 5a). All adenine bands are visible on the Fmoc-FF/Ag NP template at various concentrations from 10^{-4} to 10^{-9} M, including bands at, e.g., 735 cm^{-1} (ring breathing) and 1275 cm^{-1} (C_8–H bending, N_9–H, N_7–C_8).[33,54,55] The intensity of the adenine bands increased with increasing concentration; the intensity of the 1275 cm^{-1} band is shown in Fig. 5b.[33,54] SERS was also recorded for adenine on Ag NPs on Si and on the Fmoc-FF/Ag NP template for comparison (Fig. 5a). Fewer bands were detected on Ag NPs on Si at 10^{-6} M (Fig. S14a). The Fmoc-FF/Ag NP template enabled the detection of probe molecule concentrations as low as 10^{-10} M, distinguishing all peaks visible at higher (10^{-5} M) concentrations (Fig. S14b). While the detection limits of TMPyP and adenine have not been investigated explicitly here, we note that TMPyP and adenine peaks were detected at the lowest concentrations attempted, 10^{-12} M and 10^{-10} M, respectively, on templates prepared with a 1:1 Fmoc-FF:Ag NP volume ratio. On organic-based templates, to our knowledge, the lowest reported concentration of adenine detected is 10^{-10} M [56] whereas the lowest concentration of TMPyP detected is 10^{-15} M.[16] Adenine has previously been detected at a concentration as low as 10^{-15} M by aggregating NPs and analyte on omniphobic surfaces.[57] Characteristic SERS spectra[18,56] were also obtained

from thymine, uracil, and lysine at 10^{-9} M concentration on Fmoc-FF/Ag NP templates (Fig. S15).

The high SERS signal observed from 3D printed templates in comparison to as prepared templates is likely attributable to a confinement effect provided by 3D printing and shear induced alignment of the Fmoc-FF fibrils (Figs. 2, S2, and S12) leading to localization of the NPs. The enhanced SERS signal from 3D printed templates in comparison to Ag NPs on Si is likely attributable to the stability of the 3D printed Fmoc-FF/Ag NP template upon addition of the TMPyP solution in contrast to the Ag NPs on the Si template (Figs. S8 and S9). Other effects could influence enhancement and require further investigation to elucidate the mechanism: (i) Fmoc-FF has carboxyl and amine group that can bind with nucleobases through hydrogen bonds and potentially enhance molecule attachment;[58] and (ii) peptide based materials are reportedly pyroelectric, a property which could facilitate charge transfer processes when heated by the excitation laser.[59]

SUMMARY

By combining the plasmonic properties of Ag NPs with Fmoc-FF hydrogels, we have successfully fabricated a low-cost, aligned, and patterned template with high sensitivity to detect molecules at concentrations as low as 1 pM. We have shown that 3D printing can be used to produce a patterned and aligned structure for reproducible SERS-based sensing. The Raman signal of both TMPyP and adenine deposited on the template was found to be enhanced compared to control samples with only Ag NPs on a Si substrate. The SERS signal enhancement is attributed to the printed Fmoc-FF that support the formation of a reproducible concentration of NPs at the nanocomposite surface. The template was found to be very stable with only ~ 5 % changes in SERS intensity within and between samples. Whereas in this work, 3D printing has been used to create 2D patterns, future work exploring the potential use of 3D SERS templates can be pursued now that the suitability of the approach is established. The template described has the potential to facilitate SERS-based chemical and biomolecular detection in areas of medicine, food safety, biotechnology, and cell labelling for bio-diagnostics of diseases.

ACKNOWLEDGEMENTS

This research was funded by the Ministry of Higher Education of Saudi Arabia under the King Abdullah Scholarship Program (IR10161 and IR10133), Enterprise Ireland (CF-2016-0389-P), the European Union's Horizon 2020 research and innovation program under Marie Skłodowska-Curie grant agreement number 644175, and Science Foundation Ireland (16/IA/4584, 13/TIDA/B2701, and 12/IP/1556). This project was co-funded by the European Regional Development Fund (ERDF) under Ireland's European Structural and Investment Funds Programmes 2014-2020. The authors acknowledge Ian Reid and Aaron Martin for assistance with SEM and FTIR, respectively.

Author Contributions

The manuscript was written through contributions of all authors. All authors have given approval to the final version of the manuscript. The authors declare no competing financial interest.

References

(1) Hoffman, A. S. Hydrogels for Biomedical Applications. *Adv. Drug Delivery Rev.* **2012**, *64*, 18–23. https://doi.org/10.1016/j.addr.2012.09.010.

(2) Gaharwar, A. K.; Peppas, N. A.; Khademhosseini, A. Nanocomposite Hydrogels for Biomedical Applications. *Biotechnol. Bioeng.* **2014**, *111* (3), 441–453. https://doi.org/10.1002/bit.25160.

(3) Smith, A. M.; Williams, R. J.; Tang, C.; Coppo, P.; Collins, R. F.; Turner, M. L.; Saiani, A.; Ulijn, R. V. Fmoc-Diphenylalanine Self Assembles to a Hydrogel via a Novel Architecture Based on π–π Interlocked β-Sheets. *Adv. Mater.* **2008**, *20* (1), 37–41. https://doi.org/10.1002/adma.200701221.

(4) Zhou, M.; Smith, A. M.; Das, A. K.; Hodson, N. W.; Collins, R. F.; Ulijn, R. V.; Gough, J. E. Self-Assembled Peptide-Based Hydrogels as Scaffolds for Anchorage-Dependent Cells. *Biomaterials* **2009**, *30* (13), 2523–2530. https://doi.org/10.1016/j.biomaterials.2009.01.010.

(5) Dudukovic, N. A.; Zukoski, C. F. Gelation of Fmoc-Diphenylalanine Is a First Order Phase Transition. *Soft Matter* **2015**, *11*, 7663–7673. https://doi.org/10.1039/C5SM01399B.

(6) Yan, X.; Zhu, P.; Li, J. Self-Assembly and Application of Diphenylalanine-Based Nanostructures. *Chem. Soc. Rev.* **2010**, *39* (6), 1877–1890. https://doi.org/10.1039/b915765b.

(7) Yuan, D.; Xu, B. Heterotypic Supramolecular Hydrogels. *J. Mater. Chem. B* **2016**, *4* (34), 5638–5649. https://doi.org/10.1039/C6TB01592A.

(8) Adler-Abramovich, L.; Gazit, E. The Physical Properties of Supramolecular Peptide Assemblies: From Building Block Association to Technological Applications. *Chem. Soc. Rev.* **2014**, *43* (20), 6881–6893. https://doi.org/10.1039/c4cs00164h.

(9) Worthington, P.; Pochan, D. J.; Langhans, S. A. Peptide Hydrogels - Versatile Matrices for 3D Cell Culture in Cancer Medicine. *Front. Oncol.* **2015**, *5* (April), 92. https://doi.org/10.3389/fonc.2015.00092.

(10) Tao, K.; Levin, A.; Adler-Abramovich, L.; Gazit, E. Fmoc-Modified Amino Acids and Short Peptides: Simple Bio-Inspired Building Blocks for the Fabrication of Functional Materials. *Chem. Soc. Rev.* **2016**, *45*, 3935–3953. https://doi.org/10.1039/c5cs00889a.

(11) Ischakov, R.; Adler-Abramovich, L.; Buzhansky, L.; Shekhter, T.; Gazit, E. Peptide-Based Hydrogel Nanoparticles as Effective Drug Delivery Agents. *Bioorg. Med. Chem.* **2013**, *21* (12), 3517–3522. https://doi.org/10.1016/j.bmc.2013.03.012.

(12) Gong, Y.; Chen, X.; Lu, Y.; Yang, W. Self-Assembled Dipeptide-Gold Nanoparticle Hybrid Spheres for Highly Sensitive Amperometric Hydrogen Peroxide Biosensors. *Biosens. Bioelectron.* **2015**, *66*, 392–398. https://doi.org/10.1016/j.bios.2014.11.029.

(13) Erdogan, H.; Yilmaz, M.; Babur, E.; Duman, M.; Aydin, H. M.; Demirel, G. Fabrication of Plasmonic Nanorod-Embedded Dipeptide Microspheres via the Freeze-Quenching Method for Near-Infrared Laser-Triggered Drug-Delivery Applications.

Biomacromolecules **2016**, *17* (5), 1788–1794. https://doi.org/10.1021/acs.biomac.6b00214.
(14) Almohammed, S.; Zhang, F.; Rodriguez, B. J.; Rice, J. H. Photo-Induced Surface-Enhanced Raman Spectroscopy from a Diphenylalanine Peptide Nanotube-Metal Nanoparticle Template. *Sci. Rep.* **2018**, *8* (1), 3880. https://doi.org/10.1038/s41598-018-22269-x.
(15) Almohammed, S.; Oladapo, S. O.; Ryan, K.; Kholkin, A. L.; Rice, J. H.; Rodriguez, B. J. Wettability Gradient-Induced Alignment of Peptide Nanotubes as Templates for Biosensing Applications. *RSC Adv.* **2016**, *6* (48), 41809. https://doi.org/10.1039/C6RA05732B.
(16) Almohammed, S.; Fedele, S.; Rodriguez, B. J.; Rice, J. H. Aligned Diphenylalanine Nanotube-Silver Nanoparticle Templates for High-Sensitivity Surface-Enhanced Raman Scattering. *J. Raman Spectrosc.* **2017**, *48* (12), 1799–1807. https://doi.org/10.1002/jrs.5254.
(17) Almohammed, S.; Oladapo, S. O.; Ryan, K.; Kholkin, A. L.; Rice, J. H.; Rodriguez, B. J. Wettability Gradient-Induced Alignment of Peptide Nanotubes as Templates for Biosensing Applications. *RSC Adv.* **2016**, *6* (48). https://doi.org/10.1039/c6ra05732b.
(18) Almohammed, S.; Zhang, F.; Rodriguez, B. J.; Rice, J. H. Electric Field-Induced Chemical Surface-Enhanced Raman Spectroscopy Enhancement from Aligned Peptide Nanotube-Graphene Oxide Templates for Universal Trace Detection of Biomolecules. *J. Phys. Chem. Lett.* **2019**, *10* (8), 1878–1887. https://doi.org/10.1021/acs.jpclett.9b00436.
(19) Almohammed, S.; Tade Barwich, S.; Mitchell, A. K.; Rodriguez, B. J.; Rice, J. H. Enhanced Photocatalysis and Biomolecular Sensing with Field-Activated Nanotube-Nanoparticle Templates. *Nat. Commun.* **2019**, *10* (1), 2496. https://doi.org/10.1038/s41467-019-10393-9.
(20) Malisauskas, M.; Meskys, R.; Morozova-Roche, L. A. Ultrathin Silver Nanowires Produced by Amyloid Biotemplating. *Biotechnol. Prog.* **2008**, *24* (5), 1166–1170. https://doi.org/10.1002/btpr.49.
(21) Guo, L.; Yang, B.; Wu, D.; Tao, Y.; Kong, Y. Chiral Sensing Platform Based on the Self-Assemblies of Diphenylalanine and Oxalic Acid. *Anal. Chem.* **2018**, 90, 5451. https://doi.org/10.1021/acs.analchem.8b00762.
(22) Tao, K.; Wang, J.; Li, Y.; Xia, D.; Shan, H.; Xu, H.; Lu, J. R. Short Peptide-Directed Synthesis of One-Dimensional Platinum Nanostructures with Controllable Morphologies. *Sci. Rep.* **2013**, *3*, 2565. https://doi.org/10.1038/srep02565.
(23) Reches, M.; Gazit, E. Casting Metal Nanowires within Discrete Self-Assembled Peptide Nanotubes. *Science* **2003**, *300* (5619), 625–627. https://doi.org/10.1126/science.1082387.
(24) Dujardin, E.; Peet, C.; Stubbs, G.; Culver, J. N.; Mann, S. Organization of Metallic Nanoparticles Using Tobacco Mosaic Virus Templates. *Nano Lett.* **2003**, *3* (3), 413–417. https://doi.org/Doi 10.1021/Nl034004o.
(25) Pal, U.; Castillo López, D. N.; Carcaño-Montiel, M. G.; López-Reyes, L.; Díaz-Nuñez, P.; Peña-Rodríguez, O. Nanoparticle-Assembled Gold Microtubes Built on Fungi Templates for SERS-Based Molecular Sensing. *ACS Appl. Nano Mater.* **2019**, *2* (4), 2533–2541. https://doi.org/10.1021/acsanm.9b00443.
(26) Carny, O.; Shalev, D. E.; Gazit, E. Fabrication of Coaxial Metal Nanocables Using a Self-Assembled Peptide Nanotube Scaffold. *Nano Lett.* **2006**, *6* (8), 1594–1597.

https://doi.org/10.1021/nl060468l.
(27) Liu, R.; Wei, Y.; Zheng, J.; Zhang, H.; Sheng, Q. A Hydrogen Peroxide Sensor Based on Silver Nanoparticles Biosynthesized by Bacillus Subtilis. *Chin. J. Chem.* **2013**, *31* (12), 1519–1525. https://doi.org/10.1002/cjoc.201300487.
(28) Coman, C.; Leopold, L. F.; Rugină, O. D.; Barbu-Tudoran, L.; Leopold, N.; Tofană, M.; Socaciu, C. Green Synthesis of Gold Nanoparticles by Allium Sativum Extract and Their Assessment as SERS Substrate. *J. Nanoparticle Res.* **2014**, *16* (1), 2158. https://doi.org/10.1007/s11051-013-2158-4.
(29) Quester, K.; Avalos-Borja, M.; Vilchis-Nestor, A. R.; Camacho-López, M. A.; Castro-Longoria, E. SERS Properties of Different Sized and Shaped Gold Nanoparticles Biosynthesized under Different Environmental Conditions by Neurospora Crassa Extract. *PLoS One* **2013**, *8* (10), e77486. https://doi.org/10.1371/journal.pone.0077486.
(30) Berry, V.; Saraf, R. F. Self-Assembly of Nanoparticles on Live Bacterium: An Avenue to Fabricate Electronic Devices. *Angew. Chem., Int. Ed.* **2005**, *44* (41), 6668–6673. https://doi.org/10.1002/anie.200501711.
(31) Yang, D. P.; Chen, S.; Huang, P.; Wang, X.; Jiang, W.; Pandoli, O.; Cui, D. Bacteria-Template Synthesized Silver Microspheres with Hollow and Porous Structures as Excellent SERS Substrate. *Green Chem.* **2010**, *12* (11), 2038–2042. https://doi.org/10.1039/c0gc00431f.
(32) Wu, L.; Wang, W.; Zhang, W.; Su, H.; Liu, Q.; Gu, J.; Deng, T.; Zhang, D. Highly Sensitive, Reproducible and Uniform SERS Substrates with a High Density of Three-Dimensionally Distributed Hotspots: Gyroid-Structured Au Periodic Metallic Materials. *NPG Asia Mater.* **2018**, *10* (1), e462. https://doi.org/10.1038/am.2017.230.
(33) Chan, T.-Y.; Liu, T.-Y.; Wang, K.-S.; Tsai, K.-T.; Chen, Z.-X.; Chang, Y.-C.; Tseng, Y.-Q.; Wang, C.-H.; Wang, J.-K.; Wang, Y.-L. SERS Detection of Biomolecules by Highly Sensitive and Reproducible Raman-Enhancing Nanoparticle Array. *Nanoscale Res. Lett.* **2017**, *12* (1), 344. https://doi.org/10.1186/s11671-017-2121-x.
(34) Wu, W.; Liu, L.; Dai, Z.; Liu, J.; Yang, S.; Zhou, L.; Xiao, X.; Jiang, C.; Roy, V. A. L. Low-Cost, Disposable, Flexible and Highly Reproducible Screen Printed SERS Substrates for the Detection of Various Chemicals. *Sci. Rep.* **2015**, *5* (April), 1–10. https://doi.org/10.1038/srep10208.
(35) Fu, Q.; Zhan, Z.; Dou, J.; Zheng, X.; Xu, R.; Wu, M.; Lei, Y. Highly Reproducible and Sensitive SERS Substrates with Ag Inter-Nanoparticle Gaps of 5 Nm Fabricated by Ultrathin Aluminum Mask Technique. *ACS Appl. Mater. Interfaces* **2015**, *7* (24), 13322–13328. https://doi.org/10.1021/acsami.5b01524.
(36) Fierro-Mercado, P. M.; Hernández-Rivera, S. P. Highly Sensitive Filter Paper Substrate for SERS Trace Explosives Detection. *Int. J. Spectrosc.* **2012**, *2012*, 1–7. https://doi.org/10.1155/2012/716527.
(37) Li, S. M.; Song, Y. Highly Reproducible SERS Arrays Directly Written by Inkjet Printing. *Nanoscale* **2014**, *7*, 421–425. https://doi.org/10.1039/c4nr04656k.
(38) Wang, A. X.; Kong, X. Review of Recent Progress of Plasmonic Materials and Nano-Structures for Surface-Enhanced Raman Scattering. *Materials* **2015**, *8* (6), 3024–3052. https://doi.org/10.3390/ma8063024.
(39) Habermehl, A.; Strobel, N.; Eckstein, R.; Bolse, N.; Mertens, A.; Hernandez-Sosa, G.; Eschenbaum, C.; Lemmer, U. Lab-on-Chip, Surface-Enhanced Raman Analysis by Aerosol Jet Printing and Roll-to-Roll Hot Embossing. *Sensors* **2017**, *17* (10), 2401.

https://doi.org/10.3390/s17102401.
(40) Yu, W. W.; White, I. M. Letters to Analytical Chemistry Inkjet Printed Surface Enhanced Raman Spectroscopy Array on Cellulose Paper. *Anal. Chem.* **2010**, *82* (23), 9626–9630. https://doi.org/10.1021/ac102475k.
(41) Lee, S. Y.; Kim, S. H.; Kim, M. P.; Jeon, H. C.; Kang, H.; Kim, H. J.; Kim, B. J.; Yang, S. M. Freestanding and Arrayed Nanoporous Microcylinders for Highly Active 3D SERS Substrate. *Chem. Mater.* **2013**, *25* (12), 2421–2426. https://doi.org/10.1021/cm400298e.
(42) Wu, L. A.; Li, W. E.; Lin, D. Z.; Chen, Y. F. Three-Dimensional SERS Substrates Formed with Plasmonic Core-Satellite Nanostructures. *Sci. Rep.* **2017**, *7* (1), 1–11. https://doi.org/10.1038/s41598-017-13577-9.
(43) Lu, R.; Sha, J.; Xia, W.; Fang, Y.; Gu, L.; Wang, Y. A 3D-SERS Substrate with High Stability: Silicon Nanowire Arrays Decorated by Silver Nanoparticles. *CrystEngComm* **2013**, *15* (31), 6207. https://doi.org/10.1039/c3ce40788h.
(44) Lee, S.; Hahm, M. G.; Vajtai, R.; Hashim, D. P.; Thurakitseree, T.; Chipara, A. C.; Ajayan, P. M.; Hafner, J. H. Utilizing 3D SERS Active Volumes in Aligned Carbon Nanotube Scaffold Substrates. *Adv. Mater.* **2012**, *24* (38), 5261–5266. https://doi.org/10.1002/adma.201200645.
(45) Murphy, S. V; Atala, A. 3D Bioprinting of Tissues and Organs. *Nat. Biotechnol.* **2014**, *32* (8), 773–785. https://doi.org/10.1038/nbt.2958.
(46) Yang, H.; Leow, W. R.; Chen, X. 3D Printing of Flexible Electronic Devices. *Small Methods* **2018**, *2*, 1700259. https://doi.org/10.1002/smtd.201700259.
(47) Flowers, P. F.; Reyes, C.; Ye, S.; Kim, M. J.; Wiley, B. J. 3D Printing Electronic Components and Circuits with Conductive Thermoplastic Filament. *Addit. Manuf.* **2017**, *18*, 156–163. https://doi.org/10.1016/j.addma.2017.10.002.
(48) Finn, D. J.; Lotya, M.; Coleman, J. N. Inkjet Printing of Silver Nanowire Networks. *ACS Appl. Mater. Interfaces* **2015**, *7* (17), 9254–9261. https://doi.org/10.1021/acsami.5b01875.
(49) Calvert, P. Inkjet Printing for Materials and Devices. *Chem. Mater.* **2001**, *13* (10), 3299–3305. https://doi.org/10.1021/cm0101632.
(50) Li, Y.; Zhu, H.; Wang, Y.; Ray, U.; Zhu, S.; Dai, J.; Chen, C.; Fu, K.; Jang, S.-H.; Henderson, D.; et al. Cellulose-Nanofiber-Enabled 3D Printing of a Carbon-Nanotube Microfiber Network. *Small Methods* **2017**, *1* (10), 1700222. https://doi.org/10.1002/smtd.201700222.
(51) Alruwaili, M.; Lopez, J. A.; McCarthy, K.; Reynaud, E. G.; Rodriguez, B. J. Bio-Design and Manufacturing Liquid-Phase 3D Bioprinting of Gelatin Alginate Hydrogels : Influence of Printing Parameters on Hydrogel Line Width and Layer Height. *Bio-des. Manuf.* **2019**, https://doi.org/10.1007/s42242-019-00043-w.
(52) Fedele, S.; Hakami, M.; Murphy, A.; Pollard, R.; Rice, J.; Rice, J. Strong Coupling in Molecular Exciton-Plasmon Au Nanorod Array Systems. *Appl. Phys. Lett*. **2016**, 108, 053102. https://doi.org/10.1063/1.4941078.
(53) Wang, Y.; Zu, X.; Yi, G.; Luo, H.; Huang, H.; Song, X. Ag Nanowire-Ag Nanoparticle Hybrids for the Highly Enhanced Fluorescene Detection of Protoporphyrin IX Based on Surface Plasmon-Enhanced Fluorescence. *Chinese J. Chem.* **2016**, *34* (12), 1321–1328. https://doi.org/10.1002/cjoc.201600528.
(54) Ten, G. N.; Burova, T. G.; Baranov, V. I. Calculation and Analysis of Vibrational Spectra of Adenine – Thymine , Guanine – Cytosine , and Adenine – Uracil Complementary

Pairs in the Condensed State. *J. Appl. Spectrosc*. **2009**, *76* (1), 84–92.
(55) Madzharova, F.; Heiner, Z.; Gühlke, M.; Kneipp, J. Surface-Enhanced Hyper-Raman Spectra of Adenine, Guanine, Cytosine, Thymine, and Uracil. *J. Phys. Chem. C* **2016**, *120* (28), 15415–15423. https://doi.org/10.1021/acs.jpcc.6b02753.
(56) Almohammed, S.; Rodriguez, B. J.; Rice, J. H. Nucleobase Sensing Using Highly-Sensitive Surface-Enhanced Raman Spectroscopy Templates Comprising Organic Semiconductor Peptide Nanotubes and Metal Nanoparticles. *Sens. Bio-Sensing Res.* **2019**, *24*, 100287. https://doi.org/10.1016/j.sbsr.2019.100287.
(57) Yang, S.; Dai, X.; Stogin, B. B.; Wong, T.-S. Ultrasensitive Surface-Enhanced Raman Scattering Detection in Common Fluids. *Proc. Natl. Acad. Sci. U. S. A*. **2016**, *113* (2), 268. https://doi.org/10.1073/pnas.1518980113.
(58) Tang, C.; Smith, A. M.; Collins, R. F.; Ulijn, R. V; Saiani, A. Fmoc-Diphenylalanine Self-Assembly Mechanism Induces Apparent PKa Shifts. *Langmuir* **2009**, *25* (16), 9447–9453. https://doi.org/10.1021/la900653q.
(59) Esin, A.; Baturin, I.; Nikitin, T.; Vasilev, S.; Salehli, F.; Shur, V. Y.; Kholkin, A. L. Pyroelectric Effect and Polarization Instability in Self-Assembled Diphenylalanine Microtubes. *Appl. Phys. Lett.* **2016**, *109* (14), 142902. https://doi.org/10.1063/1.4962652.

Supporting Information

3D-Printed Peptide-Hydrogel Nanoparticle Composites for Surface-Enhanced Raman Spectroscopy Sensing

Sawsan Almohammed,[a, b] Maha Alruwaili,[a, b] Emmanuel G. Reynaud,[b, c] Gareth Redmond,[d] James H. Rice[a]* and Brian J. Rodriguez[a, b]*

[a]School of Physics, University College Dublin, Belfield, Dublin 4, Ireland
[b]Conway Institute of Biomolecular and Biomedical Research, University College Dublin, Belfield, Dublin 4, Ireland
[c]School of Biomolecular and Biomedical Science, University College Dublin, Belfield, Dublin 4, Ireland
[d]School of Chemistry, University College Dublin, Belfield, Dublin 4, Ireland

*James.Rice@ucd.ie and Brian.Rodriguez@ucd.ie

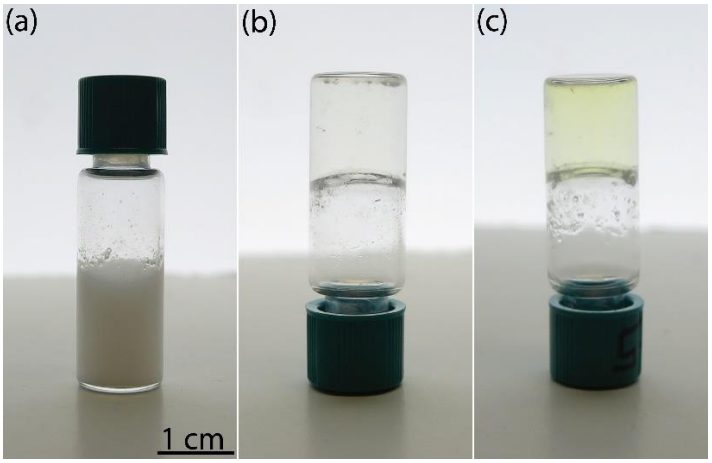

Figure S1. Images of the fluorenylmethyloxycarbonyl diphenylalanine (Fmoc-FF) hydrogels (a) immediately after adding water, (b) ~ 4 minutes later (after gelation), and (c) after adding the Ag nanoparticles (NPs).

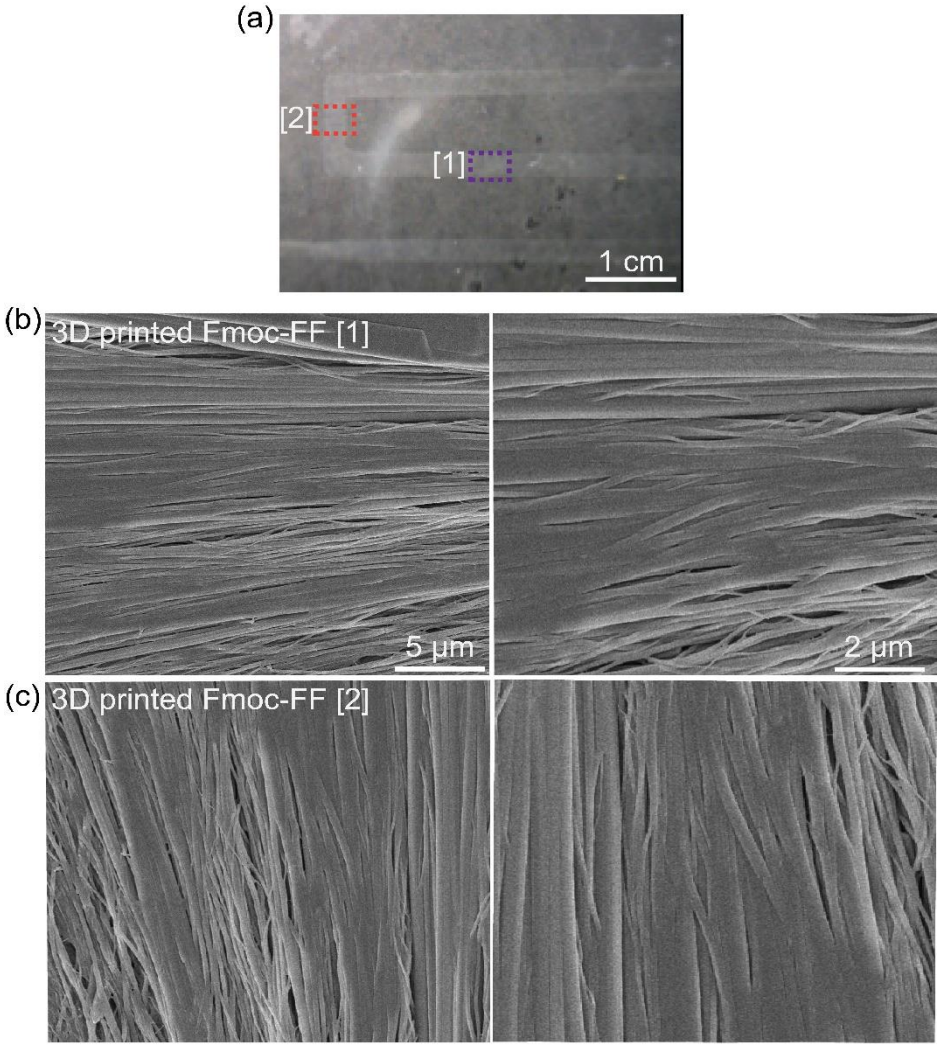

Figure S2. (a) Optical image of a three dimensional (3D) printed 2 mg/ml Fmoc-FF hydrogel on Si. Scanning electron microscopy (SEM) images at location (b) 1 and location (c) 2.

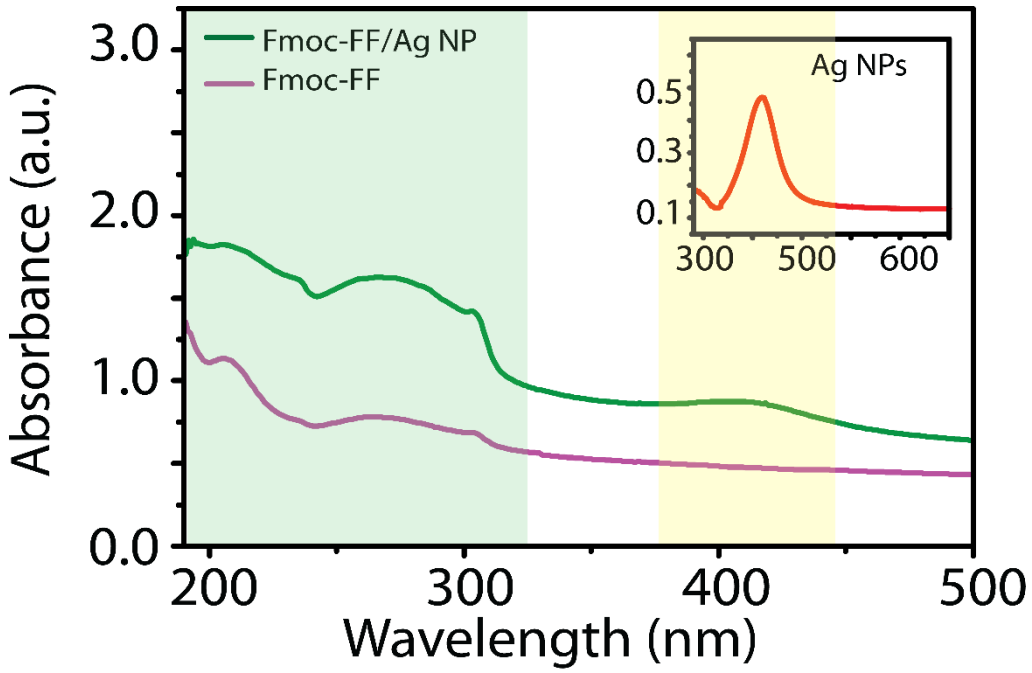

Figure S3. UV-Vis optical absorption spectra of 2 mg/ml Fmoc-FF hydrogels with and without Ag NPs. The absorption spectra of Ag NPs only in the absence of Fmoc-FF is shown in the inset. The green shading highlights Fmoc-FF bands, while the yellow shading highlights the Ag NP band.

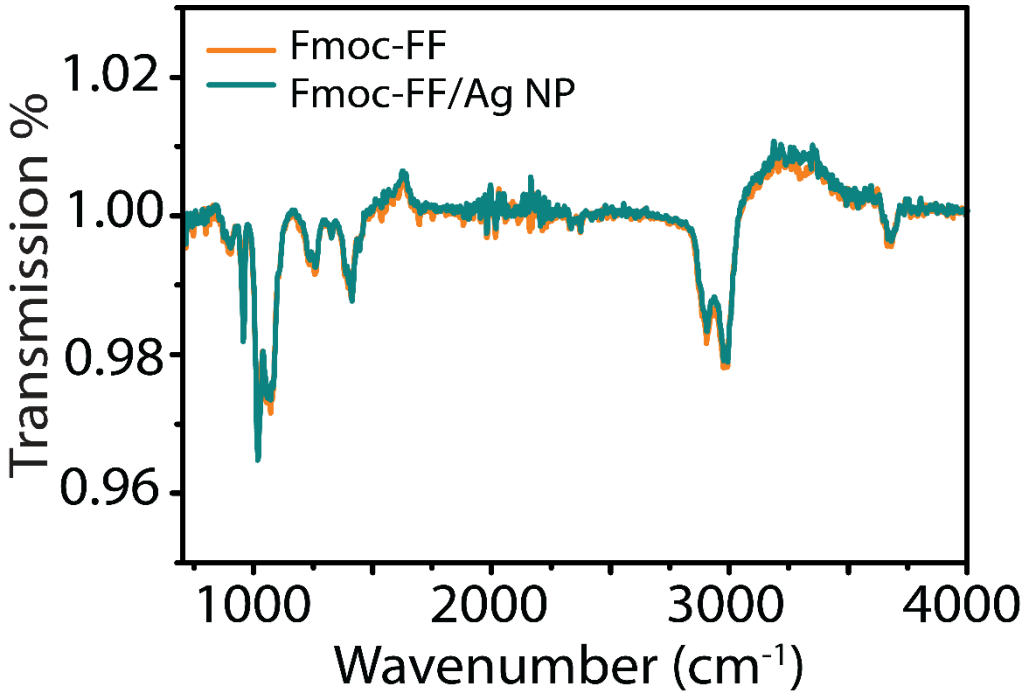

Figure S4. Fourier transform infrared spectroscopy (FTIR) spectra of a sample prepared using 2 mg/ml Fmoc-FF hydrogels with and without Ag NPs.

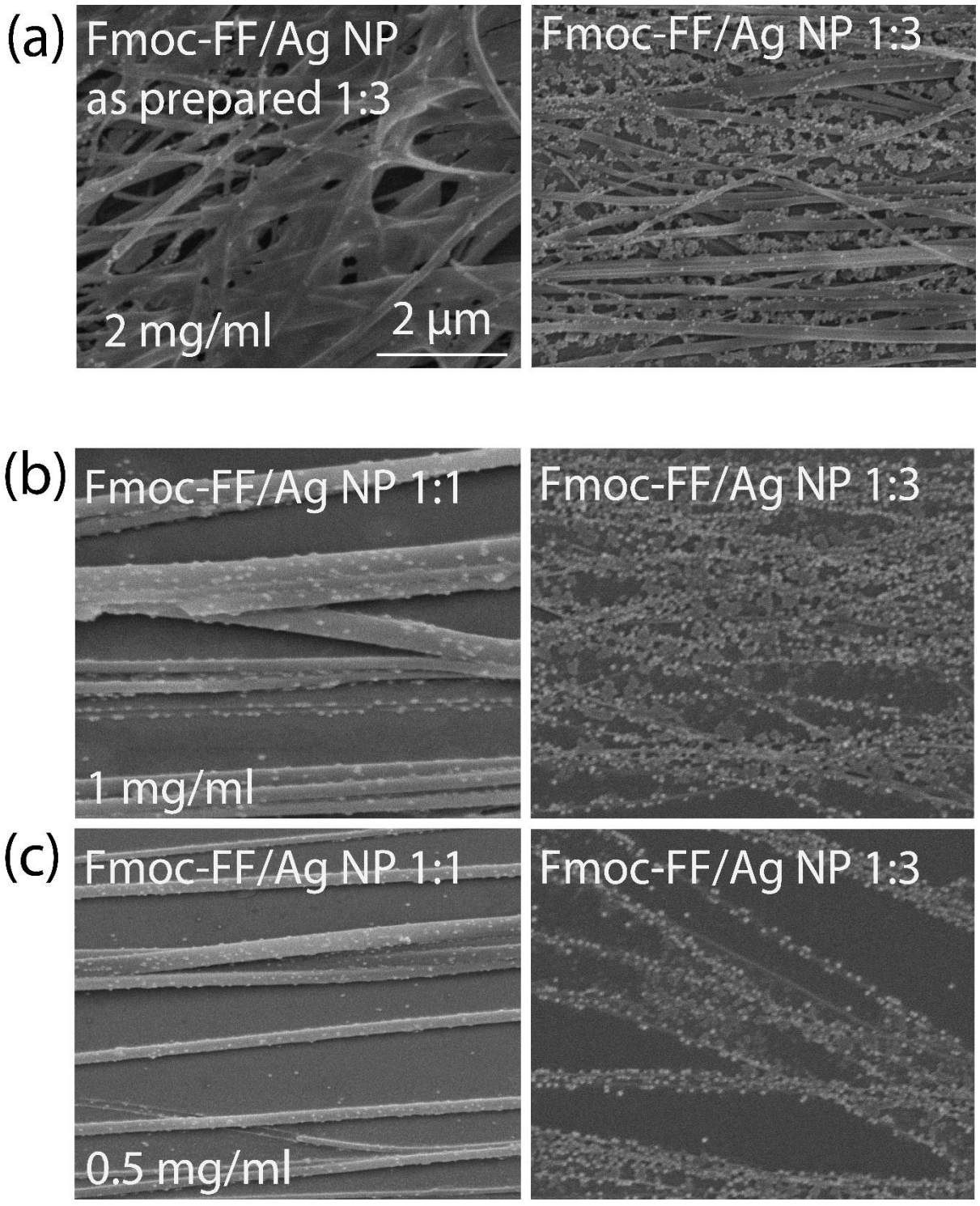

Figure S5. SEM images of (a) as prepared and 3D printed Fmoc-FF/Ag NP templates with Fmoc-FF:Ag NP volume ratios of 1:3 for an Fmoc-FF concentration of 2 mg/ml. SEM images of 3D printed Fmoc-FF/Ag NP templates with Fmoc-FF:Ag NP volume ratios of 1:1 (left) and 1:3 (right) for Fmoc-FF concentrations of (b) 1 mg/ml and (c) 0.5 mg/ml.

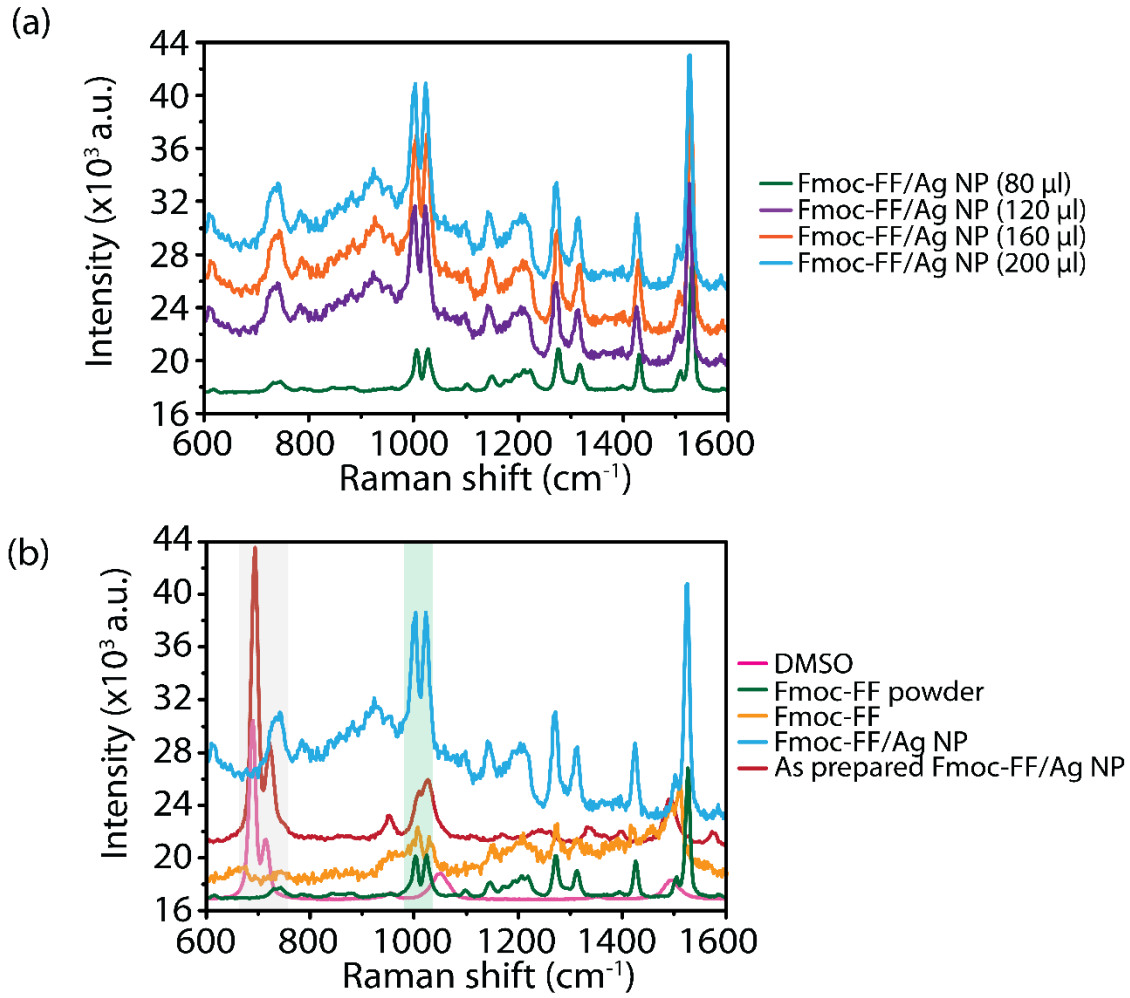

Figure S6. (a) Surface-enhanced Raman spectroscopy (SERS) spectra of 3D printed 2 mg/ml Fmoc-FF hydrogels prepared using different volumes of Ag NP solution corresponding to Fmoc-FF:Ag NP volume ratios of 25:1 (80 µl), 50:3 (120 µl), 25:2 (160 µl), and 10:1 (200 µl). (b) SERS spectra of as prepared Fmoc-FF/Ag NP (10:1; red), 3D printed Fmoc-FF hydrogel with (10:1; blue) and without (orange) Ag NPs, Fmoc-FF powder (green), and dimethyl sulfoxide (DMSO) (pink). The green shading in (b) corresponds to breathing mode bands for Fmoc-FF, whereas the gray shading highlights DMSO bands.

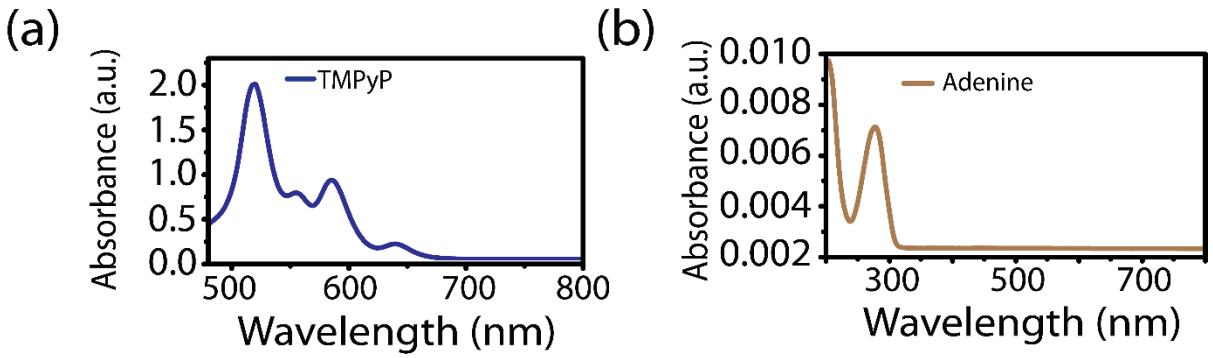

Figure S7. Ultraviolet–visible (UV-Vis) absorption spectra of 10^{-5} M (a) meso-tetra (N-methyl-4-pyridyl) porphine tetrachloride (TMPyP) and (b) adenine.

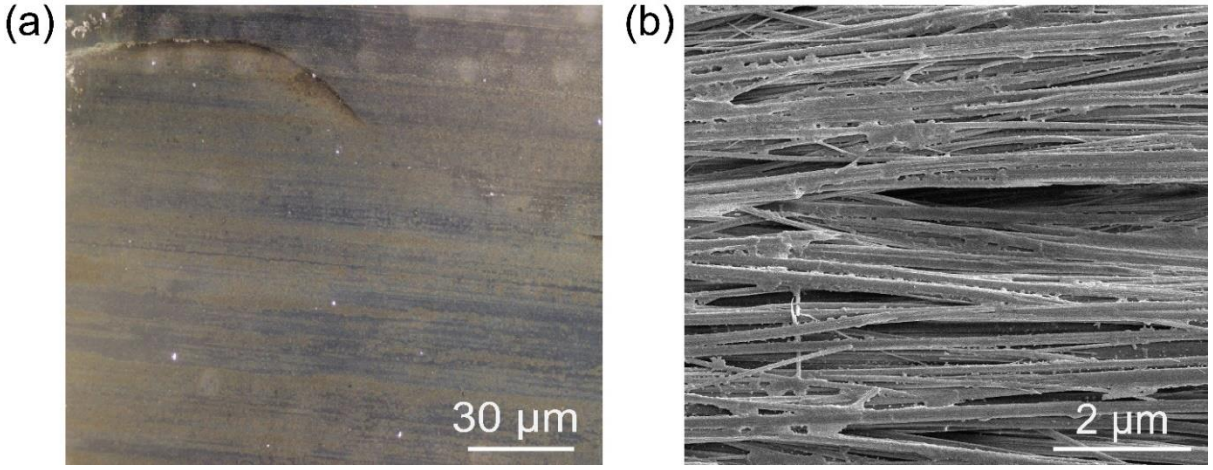

Figure S8. (a) Optical and (b) SEM images of the Fmoc-FF/Ag NP template after adding 10^{-4} M TMPyP showing that the TMPyP adheres to the template. The TMPyP solution remains confined to and spreads out on the 3D printed Fmoc-FF/Ag NP regions, as reported previously for FF peptide nanotubes,[1] apparently without dislodging the NPs.

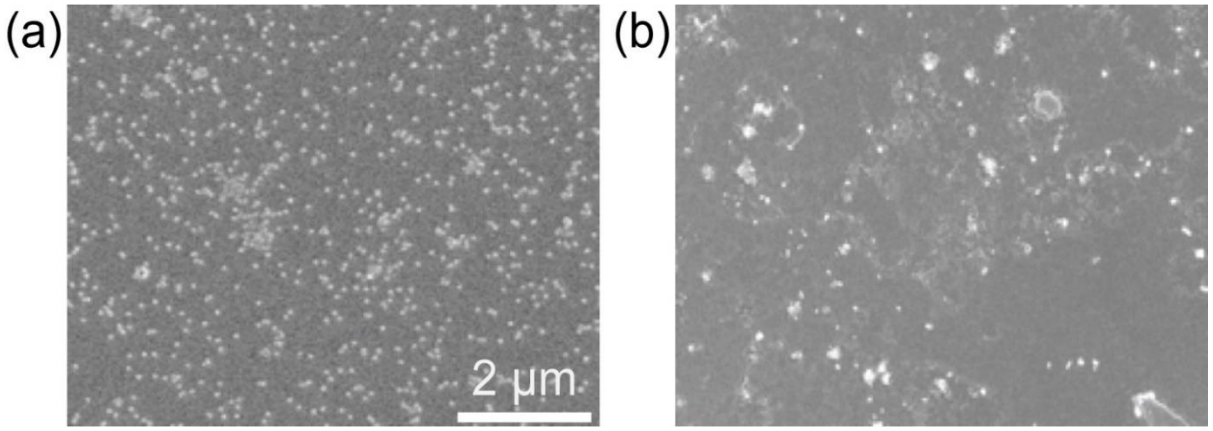

Figure S9. SEM images of Ag NPs on Si (central region) (a) before and (b) after adding TMPyP solution showing the number of NPs is reduced after the solution is added. The NP density is higher before adding TMPyP (~69 NPs/µm^2 with an interparticle spacing of ~251 nm) than afterwards (17 NPs/µm^2 with an interparticle spacing of ~606 nm).

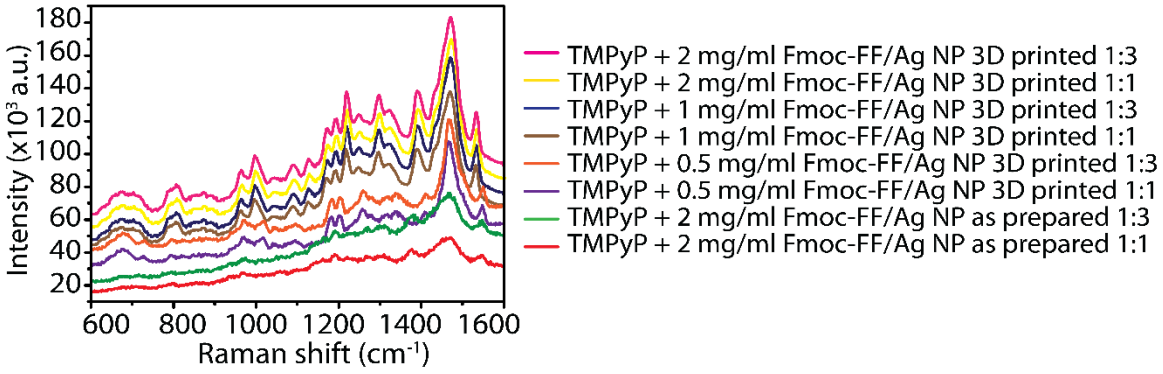

Figure S10. Surface-enhanced resonance Raman scattering (SERRS) from 10^{-5} M TMPyP on Fmoc-FF/Ag NP templates prepared with Fmoc-FF concentrations of 0.5, 1, and 2 mg/ml and Fmoc-FF:Ag NP volume ratios of 1:1 and 1:3, corresponding to the SEM images in Figure S5.

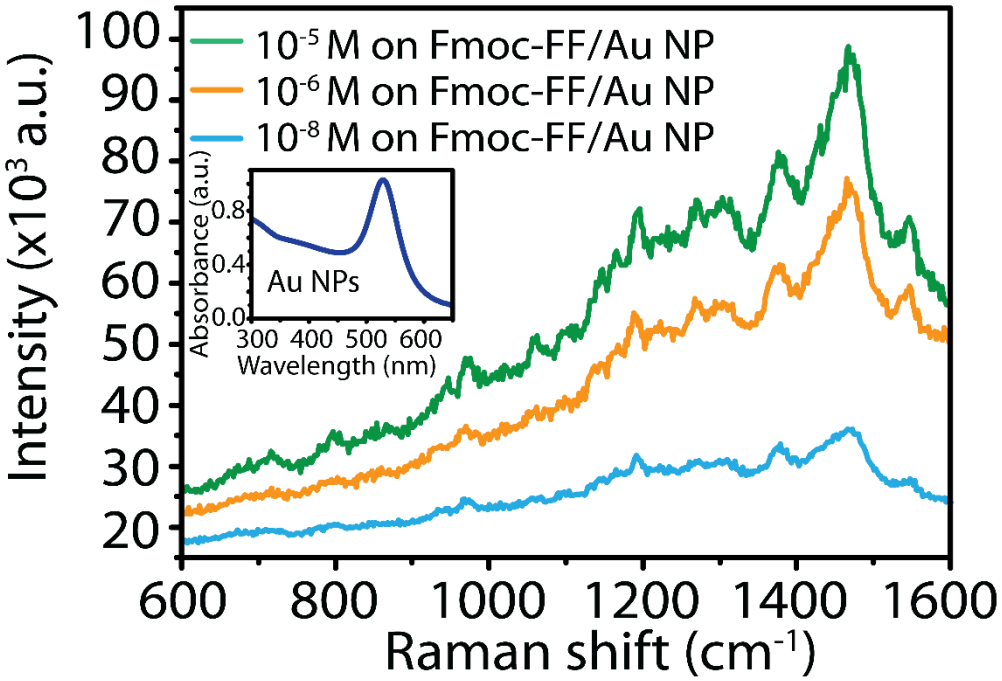

Figure S11. SERRS measurements of TMPyP on a 3D printed Fmoc-FF/Au NP template (prepared with 2 ml of Au NP solution) at different concentrations. The surface plasmon resonance of the Au NPs is around 530 nm, as shown in the inset.

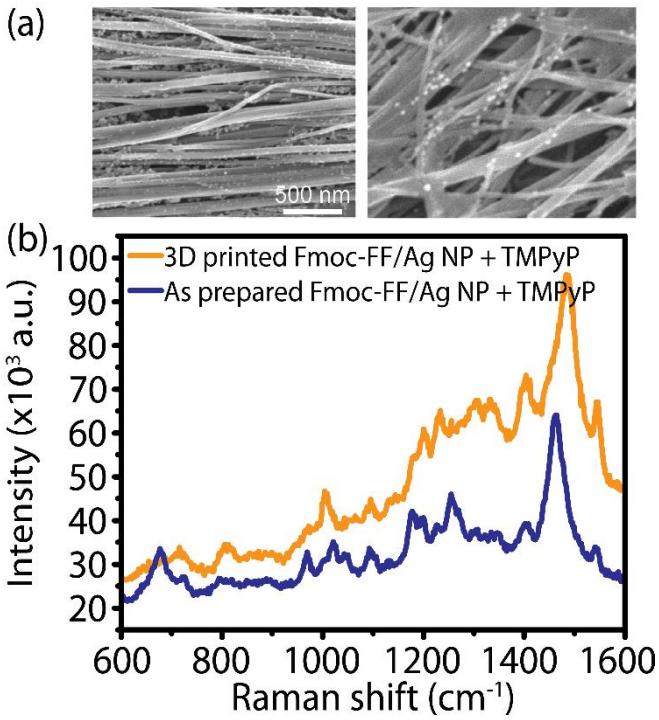

Figure S12. (a) SEM images of 3D printed (left) and as prepared (right) Fmoc-FF/Ag NP templates and (c) representative SERRS spectra for TMPyP concentrations of 10^{-6} M. The higher SERRS signal from the 3D printed template is attributed to the higher density of NPs on the 3D printed (~125 NPs/μm^2 with an interparticle spacing of ~26.5 nm) versus as prepared (~48 NPs/μm^2 with an interparticle spacing of ~155 nm) templates, based on analysis of 3 SEM images for each template. Density values are rough estimates as the number of NPs is underestimated when NPs aggregate. The NP spacing is determined as the mean measured distance between nearest NPs or NP aggregates (n = 20 pairs).

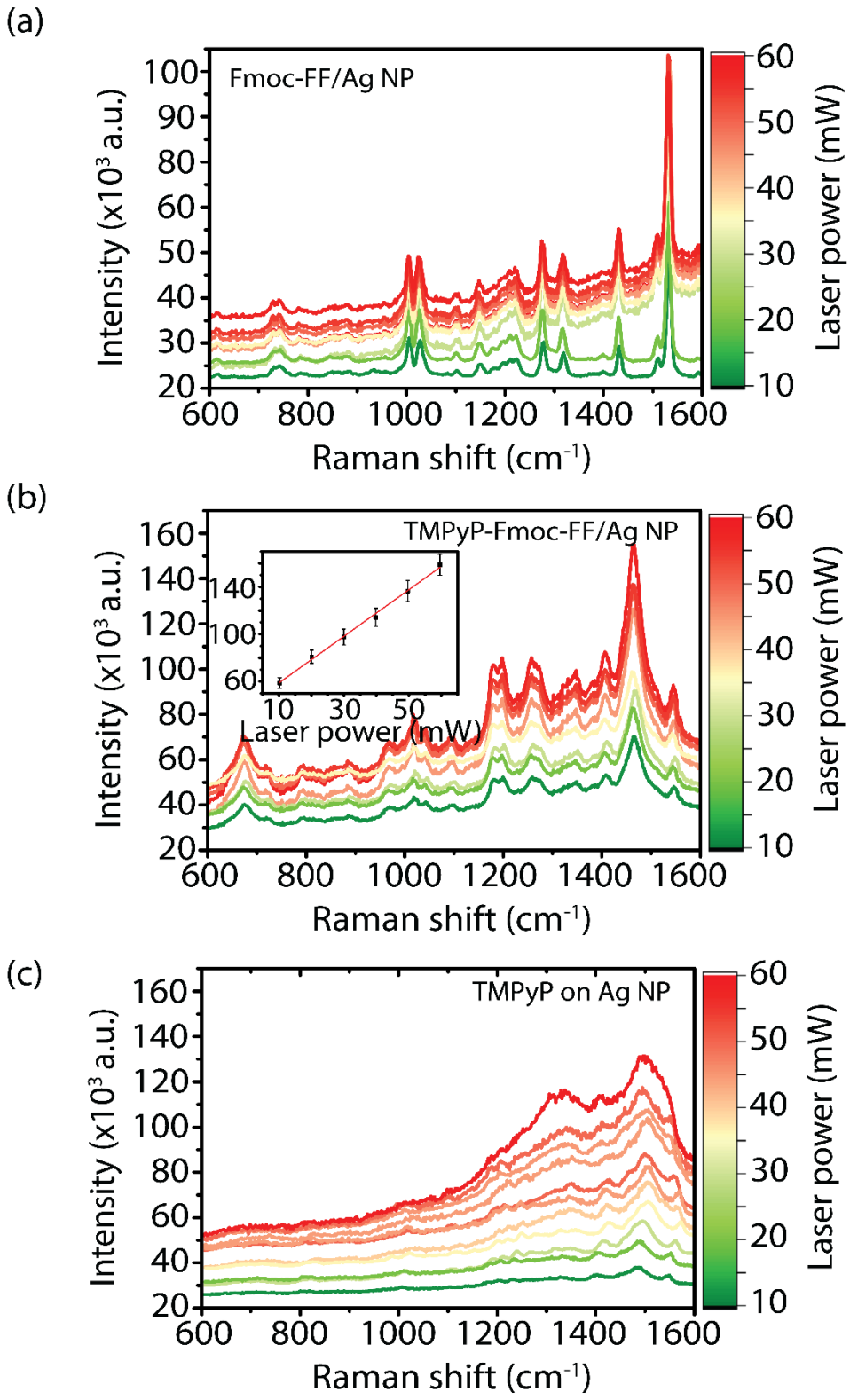

Figure S13. (a) SERS spectra of 2 mg/ml Fmoc-FF/Ag NP 3D printed templates recorded using different laser powers from 60 mW to 10 mW. (b) SERRS spectra of 10^{-5} M TMPyP on Fmoc-FF/Ag NPs 3D printed templates recorded using different laser powers from 10 mW to 60 mW. The inset in (b) shows the intensity of the 1480 cm^{-1} TMPyP band versus laser power with a linear fit. (c) SERRS spectra of 10^{-5} M TMPyP on Ag NPs only recorded using different laser powers from 10 mW to 60 mW.

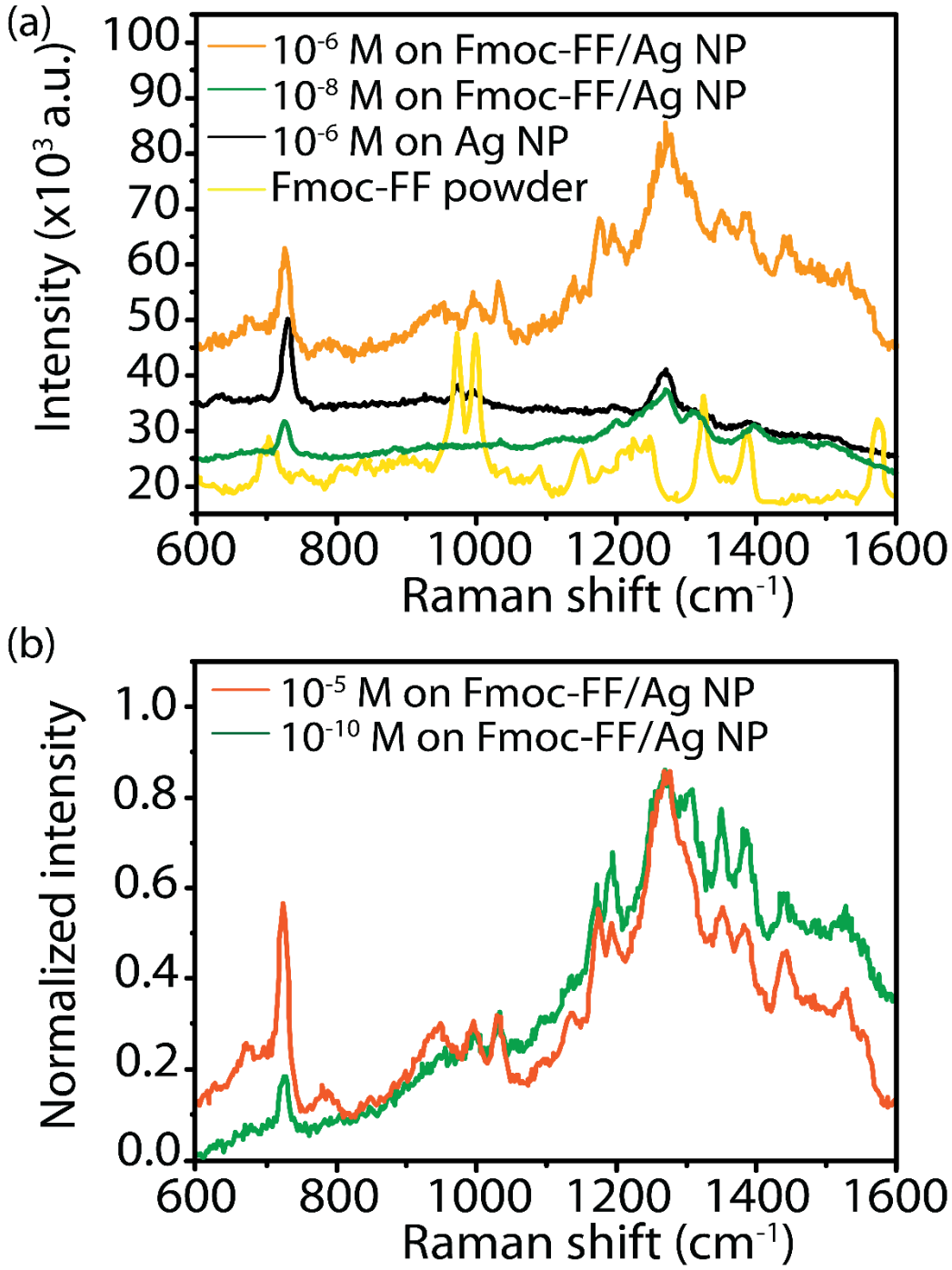

Figure S14. (a) SERS spectra from adenine on 3D printed Fmoc-FF/Ag NP templates at 10^{-6} and 10^{-8} M concentrations shown in comparison with 10^{-6} M adenine on Ag NPs alone and with Raman from Fmoc-FF powder as reference. (b) Normalized intensity SERS spectra from 10^{-5} and 10^{-10} M concentrations of adenine on 3D printed Fmoc-FF/Ag NP templates.

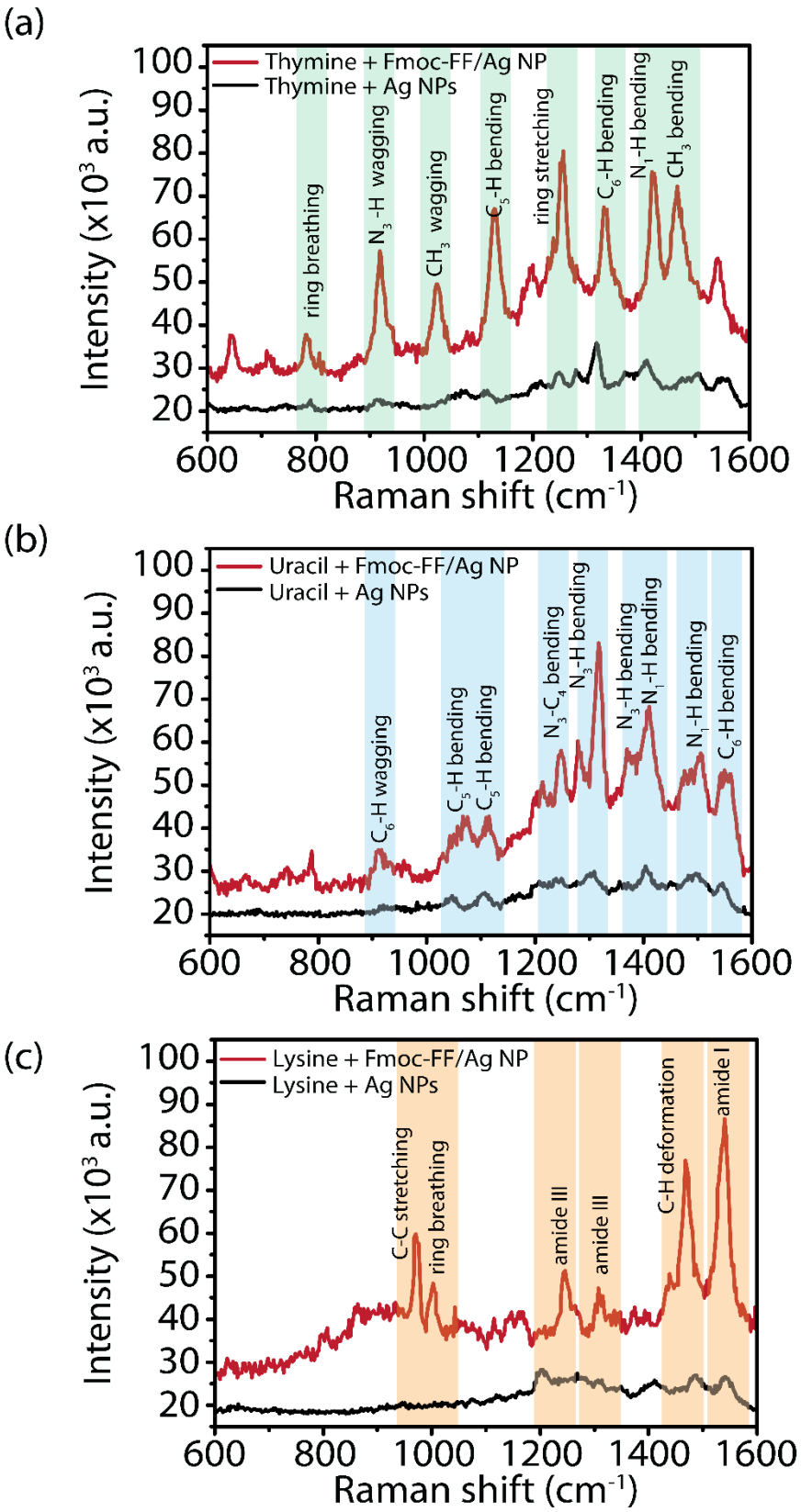

Figure S15. SERS spectra from 10^{-9} M (a) thymine, (b) uracil, and (c) lysine on 3D printed Fmoc-FF/Ag NP templates (red) versus the spectra on Ag NPs (black). Thymine, uracil, and lysine were purchased from Sigma-Aldrich and prepared as described elsewhere.[2,3]

References

(1) Almohammed, S.; Fedele, S.; Rodriguez, B. J.; Rice, J. H. Aligned diphenylalanine nanotube-silver nanoparticle templates for high-sensitivity surface-enhanced Raman scattering. *J. Raman Spectrosc.* **2017**, *48* (12), 1799–1807 DOI: 10.1002/jrs.5254.

(2) Almohammed, S.; Zhang, F.; Rodriguez, B. J.; Rice, J. H. Electric field-induced chemical surface-enhanced raman spectroscopy enhancement from aligned peptide nanotube-graphene oxide templates for universal trace detection of biomolecules. *J. Phys. Chem. Lett.* **2019**, *10* (8), 1878–1887 DOI: 10.1021/acs.jpclett.9b00436.

(3) Almohammed, S.; Rodriguez, B. J.; Rice, J. H. Nucleobase sensing using highly-sensitive surface-enhanced Raman spectroscopy templates comprising organic semiconductor peptide nanotubes and metal nanoparticles. *Sens. Bio-Sensing Res.* **2019**, *24*, 100287 DOI: 10.1016/j.sbsr.2019.100287.